

SCIENTIFIC REPORTS



OPEN

A complex pattern with hexagonal lattice and white-eye stripe in dielectric barrier discharge

Lingyan Wei, Lifang Dong, Weili Fan, Fucheng Liu, Jianyu Feng & Yuyang Pan

A novel type of white-eye pattern in a dielectric barrier discharge system has been investigated in this paper. It is a superposition of a hexagonal lattice and a white-eye stripe in appearance and evolves from a white-eye square grid state with the applied voltage increasing. Its spatio-temporal dynamics obtained by an intensified charge-coupled device shows that it consists of three transient rectangular sublattices. The spatiotemporally resolved evolutions of the molecular vibrational temperature and electron density of the pattern are measured by optical emission spectra. The evolution of surface charge distribution is given and its effect on the self-organized pattern formation is discussed.

Patterns, a kind of self-organizing phenomenon, occur in a wide range of natural contexts. Pattern formation has been studied in many different experimental systems^{1–27}, such as Faraday system^{7–10}, reaction-diffusion system^{11–13}, nonlinear optical system^{14–16} and the dielectric barrier discharge (DBD) system^{18–27}. Despite the physical differences between these systems, the patterns that appear have common features. In recent years, the study of pattern formation in the DBD system has attracted widespread attention for its many advantages. First of all, a wide variety of patterns have been found in DBD because of its high nonlinear degree. Secondly, the spatio-temporal dynamics of patterns can be easily measured by experimental method due to its self-luminous characteristics. Moreover, it has wide application prospects, such as information processing, the local growth of materials, and plasma photonic crystals^{28,29}.

The patterns can be categorized as the simple pattern and the complex pattern. Eyed patterns are a kind of complex pattern which include a special spatial structure like the naked eyes. As a significant kind of pattern types, the eyed pattern has been studied in many systems. For example, G. H. Gunaratne *et al.* gave evidence for the ‘black eye’, a simple hexagonal superlattice Turing pattern, in the chlorine dioxide-iodine-malonic acid (CDIMA) reaction³⁰. In nonlinear optical system, M. A. Vorontsov *et al.* observed the black-eye pattern which originates from interactions between spatial modes belonging to different instability bands³¹. L. F. Dong’s group has observed several white-eye patterns in a DBD system, such as the white-eye hexagonal superlattice pattern³² and the white-eye square superlattice pattern³³. Generally, the shapes of sublattices are mainly the same as the global pattern in the previous studies. For example, the ‘black eye’ pattern is a hexagonal superlattice pattern which consists of two hexagonal sublattices (black spots and white circles). The above white-eye superlattice patterns studied in DBD system are composed of three hexagonal or four square sublattices respectively. Here, a complex pattern with hexagonal lattice and white-eye stripe (CPHW) has been reported, whose sublattices’ shapes are not same as the global pattern. It is an interleaving of three rectangular transient sublattices, which is observed for the first time.

Up until now, the formation mechanism of pattern in DBD has not been well known because of its complexity. As is well known, the discharges in gas gap result in the deposition of wall charges on the surface of the dielectrics which will initiate the next discharge. Therefore, the self-organization of the pattern is indeed a self-consistent process of the discharges and the wall charges. In order to get to know the formation mechanism of pattern, the discharge and the wall charges should be measured simultaneously. Recently, the plasma states of the pattern in DBD have been studied by spectroscopic methods^{34–36}. J. H. Choi *et al.* found that the decrease in temperature induces a transition of the discharge mode by measuring the global emission spectra of He cryo-DBD³⁵. L. F. Dong *et al.* studied the electron density of an individual microdischarge channel in different stable patterns (a square and a hexagon pattern) using a spectral line profile method³⁶. In this work, the spatiotemporally resolved plasma parameters (including the molecular vibrational temperature and electron density) are measured by

College of Physics Science and Technology, Hebei University, Baoding, 071002, People’s Republic of China. Correspondence and requests for materials should be addressed to L.D. (email: donglfhbu@163.com)

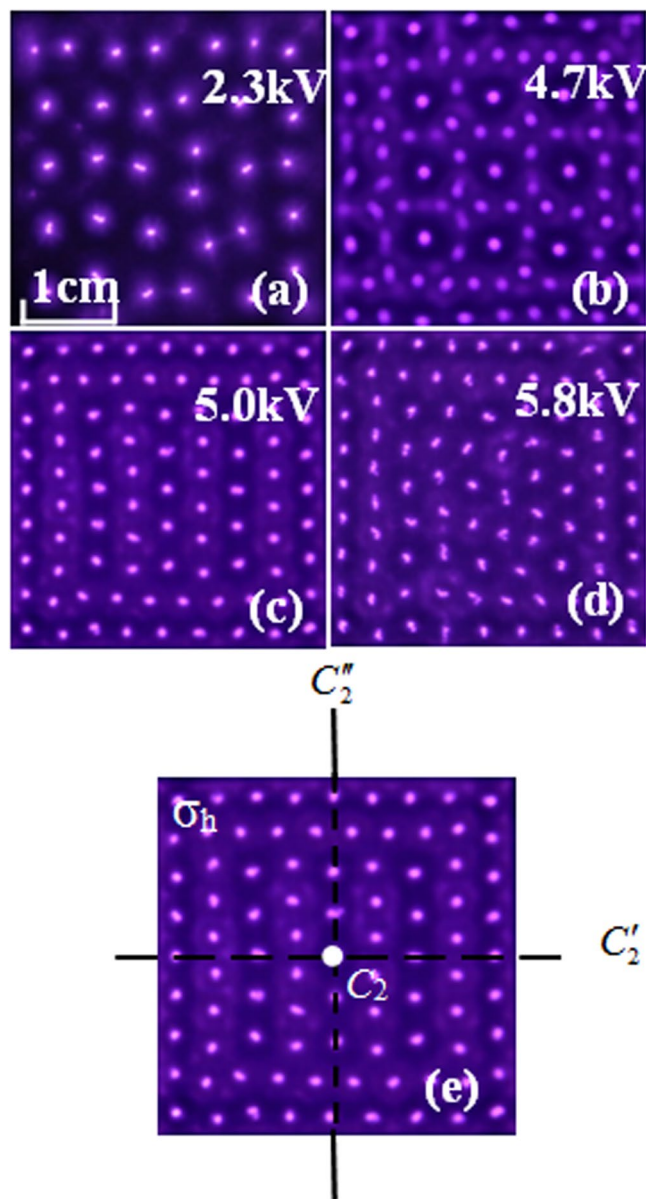


Figure 1. Evolution of patterns with increasing voltage. (a) Random filaments, $U = 2.3$ kV. (b) White-eye square grid state, $U = 4.7$ kV. (c) Complex pattern with hexagonal lattice and white-eye stripe, $U = 5.0$ kV. (d) Chaotic state, $U = 5.8$ kV. (e) The symmetric operations of (c). Other experimental parameters: gas pressure $p = 40$ kPa, argon concentration $\varphi = 50\%$, driven frequency $f = 60$ kHz, gas gap $d = 3.0$ mm, exposure time of the pictures $t = 40$ ms.

optical emission spectra and the spatio-temporal distribution of the wall charges are given based on the estimation of the electron density for the first time.

In this paper, a CPHW in a DBD system has been observed for the first time. The spatio-temporal dynamics of CPHW and white-eye square grid state (WESGS) are given. The spatiotemporally resolved evolutions of the molecular vibrational temperature and electron density of CPHW are measured by optical emission spectra. The spatio-temporal distribution of the wall charges is given and its effect on the self-organization of the pattern is discussed.

Results

The evolution of the discharge pattern. Figure 1(a–d) show the images of the pattern scenario with the applied voltage increasing. As shown in Fig. 1(c), the CPHW appears at 5.0 kV. With the increasing of the applied voltage, the pattern bifurcates from random filaments (2.3 kV), white-eye square grid state (WESGS) (4.7 kV) and finally to a chaotic state (5.8 kV). It can be seen that the CPHW is the compound of hexagonal lattice and white-eye stripe in appearance. The CPHW which has not been found in any other system enriches the pattern species.

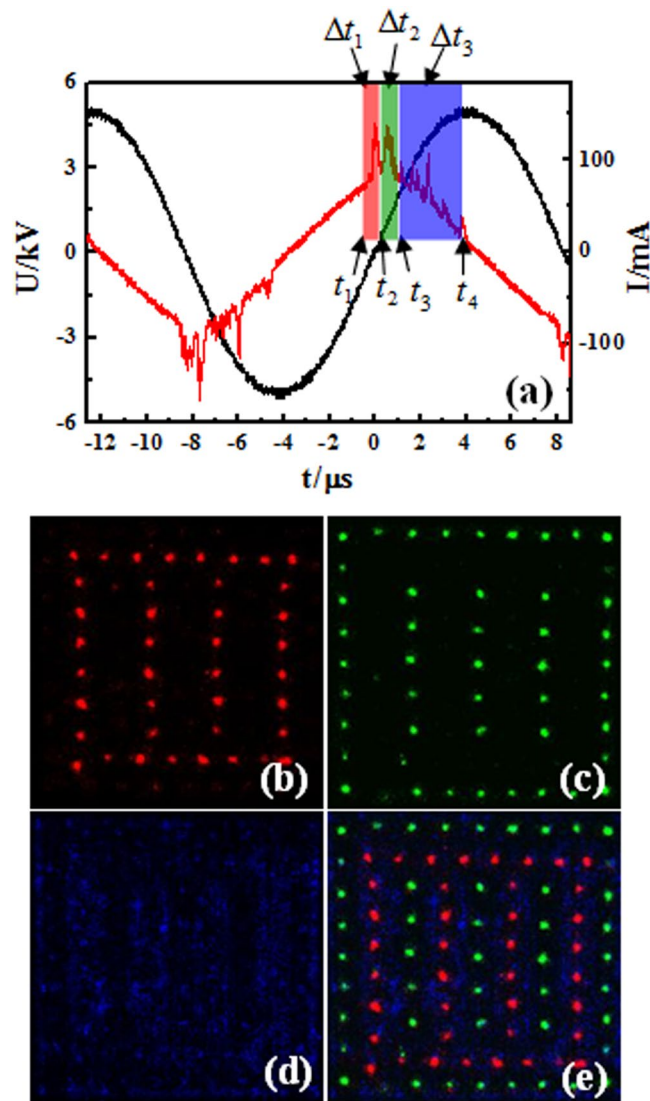


Figure 2. Instantaneous images of the complex pattern with hexagonal lattice and white-eye stripe. (a) Waveforms of the applied voltage and current of the pattern. (b) Big spots. (c) Small spots. (d) Halos. The pictures (b–d) are, respectively, correlated with current pulse phases ($\Delta t_1 = 500$ ns, $= 400$ ns, and $= 1900$ ns) in (a) and integrated over 100 voltage cycles to obtain sufficient light signals. (e) The frame is the superposition of (b, c and d).

In order to characterize the symmetry of the pattern, the corresponding point group and symmetric operations of patterns in Fig. 1(b) and (c) are analyzed. It can be seen that the WESGS belong to dihedral group D_{4h} , and the symmetric operations are $E, 5C_2, C_4, C_4^3, \sigma_h, S_4, S_4^3, i,$ and $4\sigma_v$, respectively. The CPHW belong to dihedral group D_{2h} , and symmetric operations are $E, 3C_2, \sigma_h, i,$ and $2\sigma_v$, respectively (two cyclic symmetries $2C_2$ in the principal plane, one C_2 perpendicular to the principal plane, and one horizontal mirror plane σ_h as shown in Fig. 1(e). And one identity symmetry element E , one inversion symmetry element i , and two vertical mirror planes $2\sigma_v$).

Discharge characteristic measurement of CPHW and WESGS. To explore the formation mechanism of CPHW, the instantaneous images with different exposure time are taken by an ICCD camera. Figure 2(a) presents the waveforms of the voltage and the current. Correlated with the current pulse phases ($\Delta t_1, \Delta t_2,$ and Δt_3) denoted in Fig. 2(a), instantaneous images are recorded and shown in Fig. 2(b–d), and the pictures which are integrated over 100 voltage cycles make the structures of the pattern clear. The four pictures indicate that during the first current pulse (Δt_1), which starts at the negative half voltage cycle and ends at the positive half voltage cycle, the discharge ignites in the big spots' position. Then another rectangular sublattice (small spots) is generated in Δt_2 . Finally the halos discharge in the third part of the current (Δt_3). Figure 2(e) is the superposition of (b), (c) and (d). The results show that the CPHW is composed of three transient rectangular sublattices: big spots, small spots and halos (denoted by B, S and H, respectively), and the discharge sequence is B-S-H-B-S-H within one cycle of the voltage. These three transient rectangular sublattices all belong to D_{2h} point group. The global

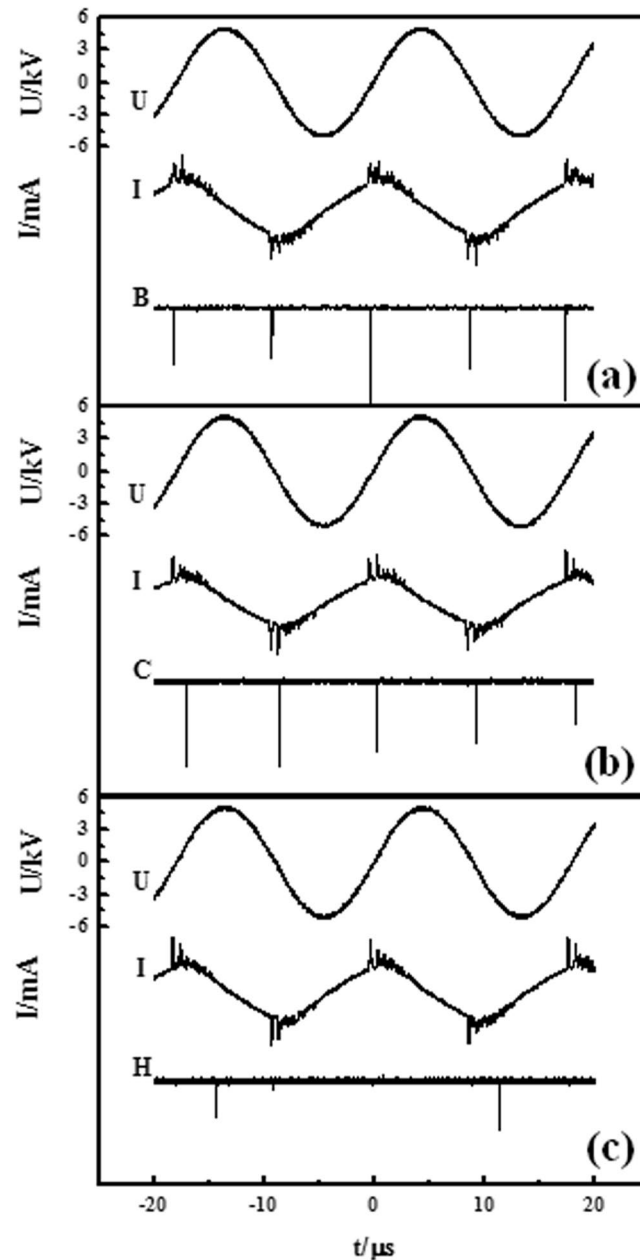


Figure 3. Time correlation measurement of the white-eye square grid state. B stands for the big spots in the center of the halos, C stands for the central spots, H stands for the halos. (a) Time correlation measurement of big spots. (b) Time correlation measurement of central spots. (c) Time correlation measurement of halos. U stands for voltage curve, I stands for current curve.

structure also belongs to D_{2h} point group although the global structure of CPHW is the compound of a hexagonal lattice and a white-eye stripe. It can be seen that the sublattices show the intrinsic symmetry feature of the global pattern.

In order to study the symmetry changes in the pattern evolution process, the temporal correlations between the filaments of WESGS are measured by a PMT. Figure 3 gives the light emissions of big spot, central spot, and part of halo (denoted by B, C, and H) respectively. It is found that the big spots with halos around are ignited simultaneously corresponding to the first pulse phase (the falling edge of the voltage) in each half driving cycle in Fig. 3(a). The central spots discharge slightly later (the rising edge of the voltage) than the big spots (Fig. 3(b)), and the halos discharge at the last part (the rising edge of the voltage) of the pulse phase (Fig. 3(c)). When a part of the halo is measured by PMT, the optical signal only appears in some half voltage cycle (Fig. 3(c)), indicating that the halo consist of several filaments (generally 3–4 filaments³⁷) whose positions are not fixed. By analogy, the halo of CPHW also consists of unfixed filaments. Thus, it can be obtained that the WESGS is an interleaving of three square sublattices, and the discharge sequence is big spots–central spots–halos in each half voltage cycle. The WESGS and its sublattices all belong to D_{4h} point group.

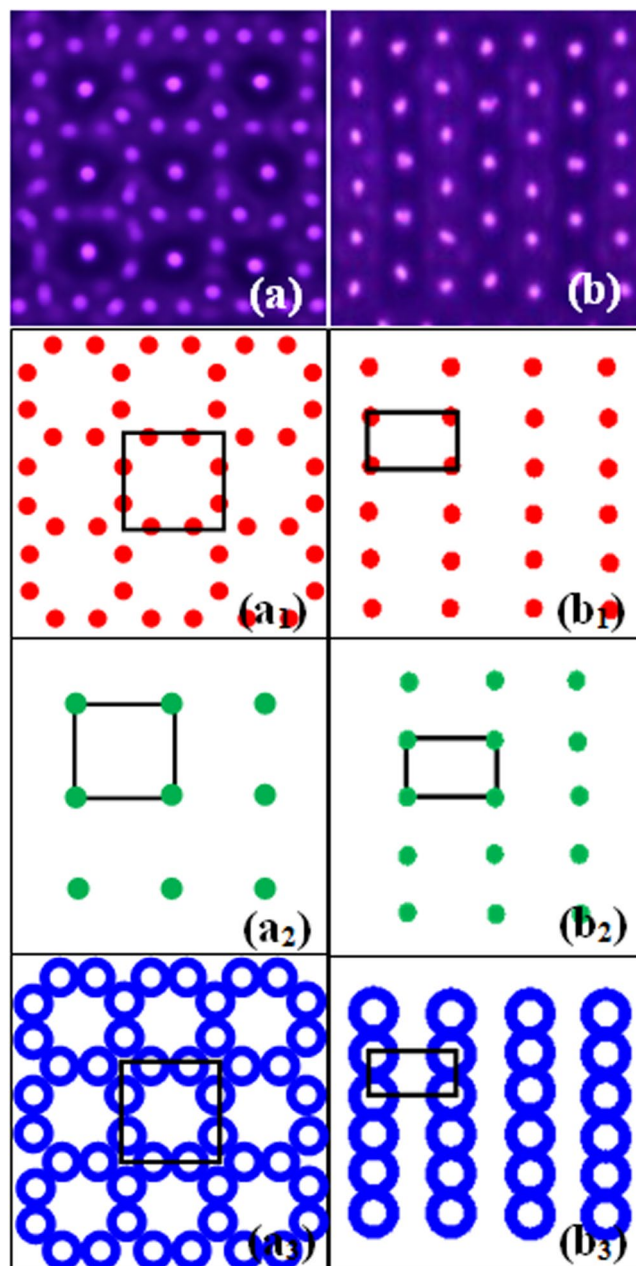


Figure 4. Schematic diagrams of the white-eye square grid state and the complex pattern with hexagonal lattice and white-eye stripe. **(a)** The white-eye square grid state. **(a₁–a₃)** Are the different sublattices of the white-eye square grid state. **(b)** The complex pattern with hexagonal lattice and white-eye stripe. **(b₁–b₃)** Are the different sublattices of the complex pattern with hexagonal lattice and white-eye stripe.

The comparison between the CPHW and the WESGS is shown in Fig. 4. It visually shows that the WESGS is an interleaving of three different square sublattices, and all of the sublattices (Fig. 4(a₁–a₃)) show the square symmetry. And the global CPHW is the compound of hexagonal lattice and white-eye stripe, but the three sublattices of CPHW all present a rectangular shape (Fig. 4(b₁–b₃)). In a word, both CPHW and WESGS have three sublattices, but their symmetry decreases from D_{4h} to D_{2h} through self-organization.

The spatiotemporally resolved OES of the CPHW. In order to study the influence of the plasma states on the pattern's self-organization process, the plasma parameters are studied by optical emission spectra (OES) (Fig. 5). As each sublattice of the CPHW discharges in the corresponding current pulse, the OES collected from any sublattice should also represent the OES of the pattern discharge during the corresponding current pulse. Therefore, the spatially resolved OES measurements of the three sublattices can also achieve the temporally resolved measurements, i.e., the spatiotemporally resolved OES of the CPHW can be obtained by collecting OES from three sublattices respectively.

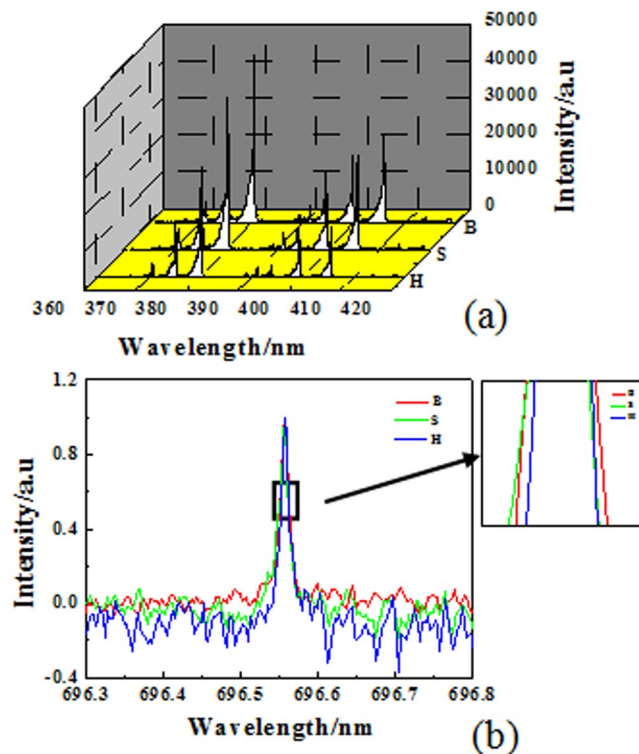


Figure 5. (a) Spectrum lines of the broadenings of N_2 second positive band system ($C^3\Pi_u \rightarrow B^3\Pi_g$) at different positions. (b) The profiles of the spectral line 696.5 nm of the three discharges sublattices.

In experiments, the OES of each sublattice is collected by using a spectrometer with an optical fiber probe. For measuring the spectrum of an individual microdischarge channel in each sublattice, the discharge pattern is magnified by a lens so that the diameter of the image of one microdischarge channel is little more than inside diameter of optical fiber probe, making sure that the emission of only one microdischarge channel is transmitted into the optical fiber probe.

Figure 5(a) gives the spectrum lines of the N_2 second positive band system ($C^3\Pi_u \rightarrow B^3\Pi_g$) of three sublattices, from which the molecular vibrational temperatures of three sublattices are calculated. After a lot of measurements, the average vibrational temperatures are (2390 ± 30) K for B, (2440 ± 30) K for S, and (2650 ± 30) K for H, respectively. The ascending order of the temperature is B-S-H.

Figure 5(b) shows the profiles of Ar I ($2P_2 \rightarrow 1S_5$) spectral line of the three different sublattices, which are obtained by selecting the 2400 groove/mm grating. Results indicate that the broadening of B, S and H is (0.014 ± 0.004) nm, (0.013 ± 0.004) nm, (0.011 ± 0.004) nm, respectively. As is well known, in plasma with electron density higher than 10^{15} cm^{-3} , the Stark effect plays an important role in the atom spectral line broadening. The electron density N_e can be estimated by Stark broadening of Ar I line ω_t through

$$\omega_t = 2 \times [1 + 1.75 \times 10^{-4} N_e^{1/4} \alpha \times (1 - 0.068 N_e^{1/6} T_e^{-1/2})] \times 10^{-16} \omega_e N_e$$

where T_e (in kelvins) is the electron temperature, ω_e is the electron impact width, and α is the ion broadening parameter³⁸. So it can be approximately obtained that the ascending order of the electron density is H-S-B.

Figure 6 shows the spatiotemporally resolved plasma parameters of the complex pattern with hexagonal lattice and white-eye stripe. It can be summarized that the big spots (B) corresponding the first pulse (Δt_1) have the lowest molecular vibrational temperature and the largest electron density. The small spots (S) corresponding the second pulse (Δt_2) have moderate molecular vibrational temperature and electron density, while the halos (H) corresponding the third pulse (Δt_3) have the highest molecular vibrational temperature and the smallest electron density. In this way, it obtains the spatiotemporally resolved plasma parameters of CPHW. The results show that the three sublattices of CPHW are in different plasma states. Generally, the surface density of wall charges can be characterized by the electron density since the discharge duration of a filament in different sublattices is almost the same. So it can be obtained that the ascending order of wall charges is H-S-B.

By comparing Fig. 2(c) and (d), it can be seen that different plasma states can lead to different self-organization processes. As mentioned above, the small spots and halos are in different plasma states. The filaments in Fig. 2(c) are fixed, while the filaments in halo in Fig. 2(d) are random. In other words, filaments of halo can not form a regular sublattice in each half cycle, but they can form regular halo sublattice in hundreds cycles. Thus the small spots sublattice is the fixed arrangement by self-organization, while the halos sublattice is the statistically outcome of self-organization. In a word, different plasma states can lead to different self-organization processes.

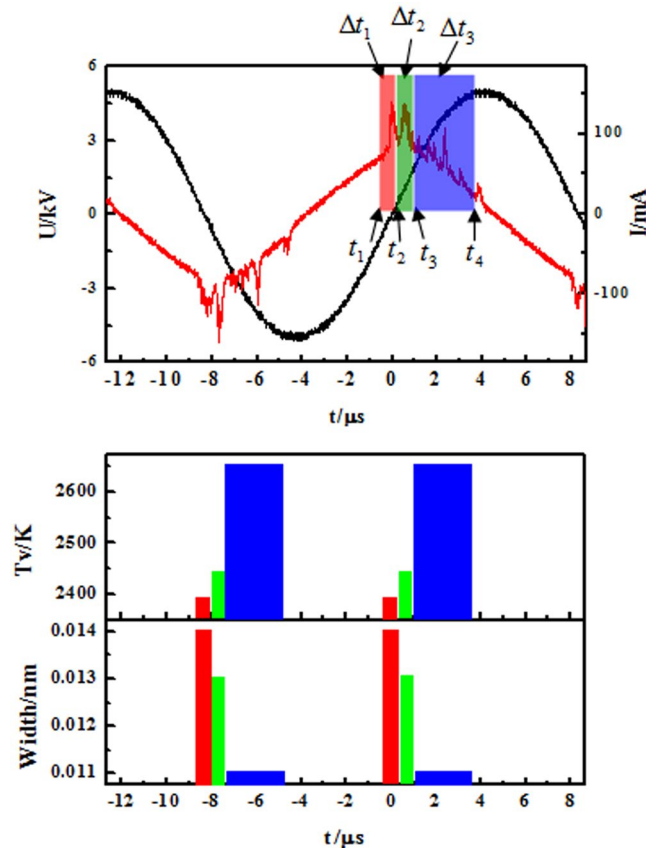


Figure 6. The spatiotemporally resolved plasma parameters of the complex pattern with hexagonal lattice and white-eye stripe.

Discussions

According to the above results, the spatio-temporal characteristics of the CPHW are analyzed in Fig. 7. The wall-charge electric fields of the big spots, small spots and halos are named E_b , E_s and E_h , respectively. The negative sign is added to E_b , E_s and E_h when they are reversed to E_{app} . The different discharge moments ($t_1 - t_4$) are marked in Fig. 7(a). At the end of one half voltage cycle (t_1), the cell of the wall charges is shown in Fig. 7(a1) and (b1) (red represents the positive charge, black represents the negative charge). It indicates that the wall-charge electric fields of all spots ($-E_b$, $-E_s$, and $-E_h$) have an opposite direction with E_{app} , and the sum fields is large enough to overcome applied voltage to reach the breakdown threshold of the big spots who have the largest wall charges. Then the big spots are reversed ignition (Fig. 7(c1)). After the big spots discharge, the status of wall-charge electric fields turns into Fig. 7(a2) and (b2). It is worth noting that E_{app} have reversed in t_2 , so did the wall-charge electric fields. The discharge continues until the rising edge of voltage which ensures the reversal of big spots' wall charges. In this discharge process, all of the wall-charge electric fields act as an activator, and the applied electric field acts as an inhibitor in the process of this discharge. Then under the influence of E_{app} , $-E_b$ and E_s , the small spots who have more wall charges than halos are ignited firstly at the rising edge of applied voltage with the voltage increasing (Fig. 7(c2)). Due to the feedback electric field is generated by wall charges accumulated on the dielectric surface, the sum of fields (E_{app} and $-E_s$) tends to decrease, which leads to discharge quenching. Each cell of the wall charges at t_3 is shown in Fig. 7(a3) and (b3). After the small spots discharge, the wall charges accumulated in the place of the small spots have a counteractive effect on surrounding. Under the effects of E_{app} , $-E_b$, and $-E_s$, the halos discharge far away from the small spots and form a shape of ring on the outside of the big spots (Fig. 7(c3)). After the halos discharge, the wall charges will be the same as that in Fig. 7(b4) and (a4). Then the applied voltage begins to decrease, and the pattern will repeat the above sequence which demonstrates the periodicity of the sequence. It's worth noting that the applied voltage plays a leading role in the discharging of small spots and halos, while the discharging of big spots is mainly effected by wall charges.

Above all, a CPHW whose sublattices' shapes are different from the global pattern has been obtained. The CPHW is an interleaving of three rectangular transient sublattices, and the discharge sequence is big spots–small spots–halos in each half voltage cycle. The spatiotemporally resolved plasma parameters of CPHW is obtained, and each discharge sublattice presents different plasma states. The plasma states affect the self-organization of the pattern.

In conclusion, a novel type of white-eye pattern which consists of three rectangular sublattices is first reported in a dielectric barrier discharge system. The complex pattern is the compound of a hexagonal lattice and a white-eye stripe in appearance. The spatio-temporal characteristics of the complex pattern show that the CPHW consists of three different rectangular sublattices. It demonstrates that the shapes of sublattices are different from

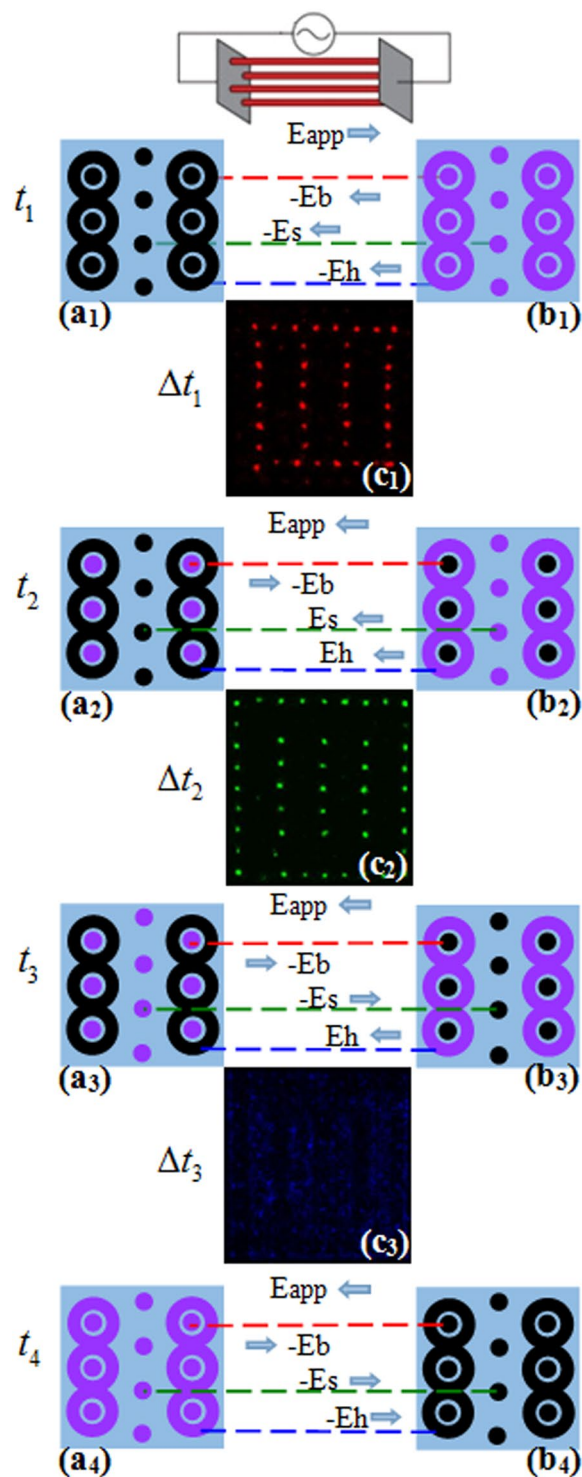


Figure 7. Time-resolved evolution sequence of the complex pattern with hexagonal lattice and white-eye stripe. (a₁–a₄) One cell of the wall charges' sublattice at different times on one side of dielectric surface. (b₁–b₄) One cell of the wall charges' sublattice at different times on the other side of dielectric surface (red represents the positive charge, black represents the negative charge). (c₁–c₃) Images corresponding over a period of time are denoted in Fig. 2(a). (c₁–c₃) Are pictures taken by ICCD camera which are integrated over 100 voltage cycles. A simplified circuit is given in the upper part of this figure. The applied electric field and the internal electric fields induced by big spots, small spots and halos are named as E_{app} , E_b , E_s and E_h , respectively. The negative sign is added to E_b , E_s and E_h when they are reversed to E_{app} .

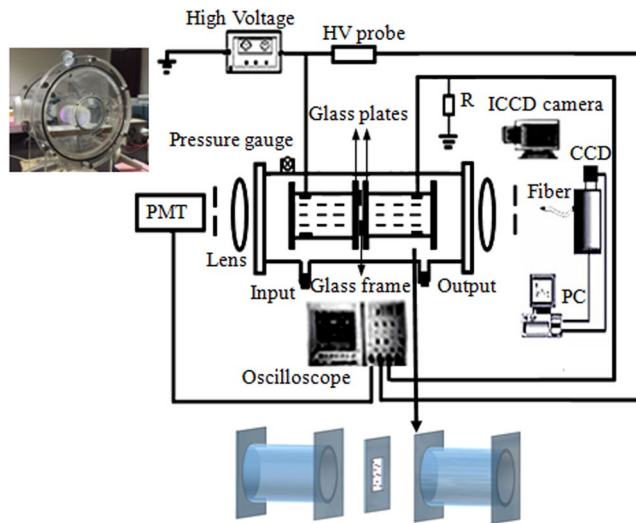


Figure 8. Schematic diagram of the experimental setup.

that of the global structure in the complex pattern. The spatiotemporally resolved evolutions of the molecular vibrational temperature and electron density of the pattern are measured by optical emission spectra. The evolution of wall charges distribution is given and its effect on the self-organization of the pattern is discussed. It is found that the plasma states affect the self-organization of the pattern. These results give insights on the underlying physics of the formation mechanism of the complex patterns in DBD.

Methods

Experimental setup. The schematic diagram of the experimental setup is shown in Fig. 8. The electrodes are two cylindrical containers which are sealed with 1.5 mm thick glass plates and filled with water. A metallic ring which is immersed in each container is used for connecting to a sinusoidal ac power supply. The ac power supply (Nanjing, China, Maoer Electronics Co., Ltd, CTP-2000K) has a fixed frequency of 60 kHz. A square glass frame with a 3 mm thickness is clamped between the two parallel glass plates, serving as a discharge gap. The whole discharge cell is enclosed in a big container where the pressure controlled in 40 kPa and filled with 50% argon and 50% air. The voltage waveform is detected by probes and recorded by a digital phosphor oscilloscope (Tektronix TDS 3054B). In circuit, the water electrodes are in series with a 50 resistor. A high-voltage probe (Tektronix P6015A 1000×) is used to detect the applied voltage. Another probe (Tektronix TPP1000) is used to detect the voltage across the resistor and the current waveform is calculated by the resistor voltage divided by the resistor. The mainly measuring instruments in this paper are intensified charge-coupled device (HSFC-PRO, 3 channels) camera, photomultiplier (PMT, ET 9085) and spectrometer (Acton Advanced SP 2750 A, CCD: 1340 × 400 pixels), respectively.

With the applied voltage increasing, filaments will form in the square glass frame between the two water electrodes. Different patterns will appear under different applied voltages (other experimental parameters: gas pressure $p = 40$ kPa, argon concentration = 50%, driven frequency $f = 60$ kHz, gas gap $d = 3.0$ mm, exposure time of the pictures $t = 40$ ms).

References

- Sharpe, J. P., Ramazza, P. L., Sungar, N. & Saunders, K. Pattern stabilization through parameter alternation in a nonlinear optical system. *Phys. Rev. Lett.* **96**, 094101, <https://doi.org/10.1103/PhysRevLett.96.094101> (2006).
- Schoenbach, K. H., Moselhy, M. & Shi, W. H. Self-organization in cathode boundary layer microdischarges. *Plasma Sources Sci. Technol.* **13**, 177–185, <https://doi.org/10.1088/0963-0252/13/1/023> (2004).
- Purwins, H. G. & Berkemeier, J. Self-organized patterns in low temperature ac gas-discharge. *IEEE Trans. Plasma Sci.* **39**, 2112–2113, <https://doi.org/10.1109/TPS.2011.2158557> (2011).
- Corr, C., Boswell, R., Balcon, N., Samuell, C. & Kenneally, P. Spatiotemporal pattern formation in an atmospheric plasma discharge. *IEEE Trans. Plasma Sci.* **36**, 964–965, <https://doi.org/10.1109/TPS.2008.924427> (2008).
- Purwins, H. G. & Stollenwerk, L. Synergetic aspects of gas-discharge: lateral patterns in dc systems with a high ohmic barrier. *Plasma Phys. Control. Fusion* **56**, 123001, <https://doi.org/10.1088/0741-3335/56/12/123001> (2014).
- Trelles, J. P. Pattern Formation and Self-Organization in Plasmas interacting with Surfaces. *J. Phys. D: Appl. Phys.* **49**, 393002, <https://doi.org/10.1088/0022-3727/49/39/393002> (2016).
- Arbell, H. & Fineberg, J. Pattern formation in two-frequency forced parametric waves. *Phys. Rev. E.* **65**, 036224, <https://doi.org/10.1103/PhysRevE.65.036224> (2002).
- Topaz, C. M., Porter, J. & Silber, M. Multifrequency control of Faraday wave patterns. *Phys. Rev. E* **70**, 066206, <https://doi.org/10.1103/PhysRevE.70.066206> (2004).
- Wagner, C., Muller, H. W. & Knorr, K. Pattern formation at the bicritical point of the Faraday instability. *Phys. Rev. E* **68**, 066204, <https://doi.org/10.1103/PhysRevE.68.066204> (2003).
- Perinet, N., Juric, D. & Tuckerman, L. S. Alternating hexagonal and striped patterns in faraday surface waves. *Phys. Rev. Lett.* **109**, 164501, <https://doi.org/10.1103/PhysRevLett.109.164501> (2012).
- Hecht, I., Kessler, D. A. & Levine, H. Transient localized patterns in noise-driven reaction-diffusion systems. *Phys. Rev. Lett.* **104**, 158301, <https://doi.org/10.1103/PhysRevLett.104.158301> (2010).
- Yang, G. X. & Xu, J. Analysis of spatiotemporal patterns in a single species reaction-diffusion model with spatiotemporal delay. *Nonlinear Anal. RWA* **22**, 54–65, <https://doi.org/10.1016/j.nonrwa.2014.07.013> (2015).

13. Yang, L. F., Zhabotinsky, A. M. & Epstein, I. R. Stable squares and other oscillatory Turing patterns in a reaction-diffusion model. *Phys. Rev. Lett.* **92**, 198303, <https://doi.org/10.1103/PhysRevLett.92.198303> (2004).
14. Louvergneaux, E., Rogister, F. & Glorieux, P. Spatiotemporal antiphase dynamics in coupled extended optical media. *Phys. Rev. Lett.* **99**, 263901, <https://doi.org/10.1103/PhysRevLett.99.263901> (2007).
15. Residori, S., Petrossian, A. & Gil, L. Sum-frequency generation in dissipative system: Experimental evidence for optical wave patterns. *Phys. Rev. Lett.* **88**, 233901, <https://doi.org/10.1103/PhysRevLett.88.233901> (2002).
16. Bortolozzo, U., Villoresi, P. & Ramazza, P. L. Experimental evidence for detuning induced pattern selection in nonlinear optics. *Phys. Rev. Lett.* **87**, 274102, <https://doi.org/10.1103/PhysRevLett.87.274102> (2001).
17. Gurevich, E. L., Zanin, A. L., Moskalenko, A. S. & Purwins, H. G. Concentric-ring patterns in a dielectric barrier discharge system. *Phys. Rev. Lett.* **91**, 154501, <https://doi.org/10.1103/PhysRevLett.91.154501> (2003).
18. Callegari, T., Bernecker, B. & Boeuf, J. P. Pattern formation and dynamics of plasma filaments in dielectric barrier discharges. *Plasma Sources Sci. Technol.* **23**, 054003, <https://doi.org/10.1088/0963-0252/23/5/054003> (2014).
19. Guikema, J., Miller, N., Niehof, J., Klein, M. & Walhout, M. Spontaneous pattern formation in an effectively one-dimensional dielectric barrier discharge system. *Phys. Rev. Lett.* **85**, 3817, <https://doi.org/10.1103/PhysRevLett.85.3817> (2000).
20. Dong, L. F. *et al.* Hexagon and square patterned air discharges. *Appl. Phys. Lett.* **90**, 031504, <https://doi.org/10.1063/1.2432950> (2007).
21. Bernecker, B., Callegari, T., Blanco, S., Fournier, R. & Boeuf, J. P. Hexagonal and honeycomb structures in dielectric barrier discharges. *Eur. Phys. J. Appl. Phys.* **47**, 22808, <https://doi.org/10.1051/epjap/2009082> (2009).
22. Dong, L. F., Li, B., Lu, N., Li, X. C. & Shen, Z. K. Hexagonal superlattice pattern consisting of colliding filament pairs in a dielectric barrier discharge. *Phys. Plasmas*. **19**, 052304, <https://doi.org/10.1063/1.4717466> (2012).
23. Zhu, P. *et al.* Honeycomb superlattice pattern in a dielectric barrier discharge in argon/air. *Phys. Plasmas*. **22**, 023507, <https://doi.org/10.1063/1.4907902> (2015).
24. Nie, Q. Y. *et al.* Self-organized pattern formation of an atmospheric pressure plasma jet in a dielectric barrier discharge configuration. *Phys. Rev. Lett.* **90**(221504), 90.221504, <https://doi.org/10.1063/PhysRevLett.90.221504> (2007).
25. Sinclair, J. & Walhout, M. Dielectric-barrier discharges in two-dimensional lattice potentials. *Phys. Rev. Lett.* **108**, 035005, <https://doi.org/10.1103/PhysRevLett.108.035005> (2012).
26. Gurevich, E. L., Zanin, A. L., Moskalenko, A. S., Bödeker, H. U. & Purwins, H. G. Rotating hexagonal pattern in a dielectric barrier discharge system. *Phys. Rev. E* **70**, 036202, <https://doi.org/10.1103/PhysRevE.70.036202> (2004).
27. Duan, X. X., He, F. & Ouyang, J. T. Various plasma patterns in planar dielectric-barrier discharge. *IEEE Trans. Plasma Sci.* **36**, 1332–1333, <https://doi.org/10.1109/TPS.2008.923833> (2008).
28. Kogelschatz, U. Filamentary, patterned, and diffuse barrier discharges. *IEEE Trans. Plasma Sci.* **30**, 1400, <https://doi.org/10.1109/TPS.2002.804201> (2002).
29. Sakaguchi, T., Sakaia, O. & Tachibana, K. Photonic bands in two-dimensional microplasma arrays. II. *Band gaps observed in millimeter and subterahertz ranges*. *J. Appl. Phys.* **101**, 073305, <https://doi.org/10.1063/1.2713940> (2007).
30. Gunaratne, G. H., Ouyang, Q. & Swinney, H. L. Pattern formation in the presence of symmetries. *Phys. Rev. E* **50**, 2802–2820, <https://doi.org/10.1103/PhysRevE.50.2802> (1994).
31. Vorontsov, M. A. & Samson, B. A. Nonlinear dynamics in an optical system with controlled two-dimensional feedback: Black-eye patterns and related phenomena. *Phys. Rev. A* **57**, 3040–3049, <https://doi.org/10.1103/PhysRevA.57.3040> (1998).
32. Dong, L. F., Shen, Z. K., Li, B. & Bai, Z. G. Pattern formation based on the triple-layer coupling mechanism. *Phys. Rev. E* **87**, 042914, <https://doi.org/10.1103/PhysRevE.87.042914> (2013).
33. Wei, L. Y. *et al.* Spatio-temporal dynamics of the white-eye square superlattice pattern in dielectric barrier discharge. *J. Phys. D: Appl. Phys.* **49**, 185203, <https://doi.org/10.1088/0022-3727/49/18/185203> (2016).
34. Stauss, S. *et al.* Uniform, Filamentary, and Striped Patterns in Helium Dielectric Barrier Discharge Cryoplasmas. *IEEE Trans. on Plasma Sci.* **39**, 2184–2185, <https://doi.org/10.1109/TPS.2011.2158857> (2011).
35. Choi, J. H., Noma, Y., Sano, M. & Terashima, K. Analysis of time-resolved optical emission of He cryoplasma at atmospheric pressure. *J. Phys. D: Appl. Phys.* **43**, 072001, <https://doi.org/10.1088/0022-3727/43/7/072001> (2010).
36. Dong, L. F., Qi, Y. Y., Zhao, Z. C. & Li, Y. H. Electron density of an individual microdischarge channel in patterns in a dielectric barrier discharge at atmospheric pressure. *Plasma Sources Sci. Technol.* **17**, 015015, <https://doi.org/10.1088/0963-0252/17/1/015015> (2008).
37. Zhao, Y., Dong, L. F., Wang, Y. J., Fu, H. Y. & Gao, Y. N. White-Eye Hexagonal Pattern in Dielectric Barrier Discharge. *J. Phys. Soc. Jpn.* **83**, 124501, <https://doi.org/10.7566/JPSJ.83.124501> (2014).
38. Griem, H. R. Plasma Spectroscopy. *New York: Mc Graw-Hill* **33**(10), 864–865 (1964).

Acknowledgements

This work was supported by the National Natural Science Foundation of China under Grant No. 11375051, Key Basic Research Project in the application basic research plan of Hebei Province under Grant No. 15961105D and the Research Foundation of Education Bureau of Hebei Province, China, under Grant No. LJRC011.

Author Contributions

Lingyan Wei and Lifang Dong wrote the main manuscript text and Jianyu Feng helped to prepare Figs 2 and 5. Weili Fan, Fucheng Liu and Yuyang Pan reviewed the manuscript.

Additional Information

Competing Interests: The authors declare no competing interests.

Publisher's note: Springer Nature remains neutral with regard to jurisdictional claims in published maps and institutional affiliations.



Open Access This article is licensed under a Creative Commons Attribution 4.0 International License, which permits use, sharing, adaptation, distribution and reproduction in any medium or format, as long as you give appropriate credit to the original author(s) and the source, provide a link to the Creative Commons license, and indicate if changes were made. The images or other third party material in this article are included in the article's Creative Commons license, unless indicated otherwise in a credit line to the material. If material is not included in the article's Creative Commons license and your intended use is not permitted by statutory regulation or exceeds the permitted use, you will need to obtain permission directly from the copyright holder. To view a copy of this license, visit <http://creativecommons.org/licenses/by/4.0/>.

© The Author(s) 2018